Time-Resolved Fluorescence Resonance Energy Transfer Study Shows a Compact Denatured State of the B Domain of Protein A[†]

F. Huang,[‡,§] E. Lerner,[‡,||] S. Sato,[§] D. Amir,[||] E. Haas,*[,||] and A. R. Fersht*[,§]

MRC Center for Protein Engineering, Hills Road, Cambridge CB2 0QH, United Kingdom, and The Goodman Faculty of Life Sciences, Bar-Ilan University, Ramat Gan, Israel 52900

Received October 7, 2008; Revised Manuscript Received February 13, 2009

ABSTRACT: The B domain of protein A (BDPA), a three-helix bundle of 60 residues, folds via a nucleation−condensation mechanism in apparent two-state kinetics. We have applied a time-resolved FRET (tr-FRET) approach to characterize the ensembles of BDPA during chemical denaturation. The distribution of the distance between residues 22 and 55, which are close and separated by helices 2 and 3 in the native state, was determined by global analysis of the time-resolved fluorescence decay curves of the probes. Narrow distributions were observed when the protein was equilibrated in guanidinium chloride (GdmCl) concentrations below 1.5 M (native state, N) and above the transition zone at 2.6−3.0 M GdmCl (denatured state, D). Considerably broader distributions were found around the transition point (2.0 M GdmCl) or much higher GdmCl concentrations (>3.0 M). Comparative global analysis of the tr-FRET data showed a compact denatured state of the protein, characterized by narrow distribution and relatively small mean distance between residues 22 and 55 that was observed at mild denaturing conditions (<3 M GdmCl). This experiment supports the two-state folding mechanism of BDPA and indicates the existence of effective nonlocal, probably hydrophobic, intramolecular interactions that stabilize a pretty uniform ensemble of compact denatured molecules at intermediate denaturing conditions.

The folding mechanisms of small single domain proteins are of considerable interest both experimentally and theoretically, since these domains can fold very rapidly in microseconds or less so that direct comparison of simulation and experiment is possible (*1*−*6*). The B domain of protein A (BDPA),[1] for example, which folds at 10^5 s^{-1} at 25 °C, has been extensively studied by theory, simulation, and experiment. BDPA is a 60-residue three-helix bundle, with helix 1 (H1, residues 10−19), turn 1 (T1, residues 20−24), helix 2 (H2, residues 25−37), turn 2 (T2, residues 38−41), and helix 3 (H3, residues 42−58). A thorough Φ-value analysis shows that this protein folds through a nucleation-condensation mechanism, with H2 being the nucleus in the transition state, although H3 seems to be more stable and has some α-helical secondary structure in the denatured state (*6, 7*). Temperature dependent Φ-value analysis further suggests that BDPA folds via a single dominant folding pathway (*8*). Single-molecule fluorescence resonance energy transfer (SM-FRET) spectroscopy has afforded direct observation of the denatured and native states of BDPA in mildly denaturing conditions (*9*).

Distributions of structural parameters that characterize the conformations of proteins under various conditions and their change with environment are essential information for understanding protein properties and folding mechanism. Unlike folded proteins, denatured (or natively disordered) proteins do not have well-defined structure and, therefore, are hard to characterize. These states are ensembles of multiple conformations, which are distinguished by distributions of intramolecular distances or coordinates and the dynamics of their changes. NMR techniques such as paramagnetic relaxation enhancement (PRE) and residual dipolar coupling (RDC) have been applied to extract information on long distance interaction and conformational distribution (*10*−*14*). Other techniques that have been applied to describe the properties of disordered proteins include small-angle X-ray scattering (SAXS) (*15*) and time-resolved fluorescence resonance energy transfer (tr-FRET) (*16, 17*). FRET can be applied to measure the distance between fluorophores due to the strong distance dependence of FRET efficiency (*18*−*21*). By measuring time-resolved fluorescence, tr-FRET can provide more information than steady-state FRET, where steady-state fluorescence intensity is measured, since the shape of the fluorescence decay curve does not depend only on the average distance between the donor and the acceptor but also depends on their distance distribution and fluctuations (*22*).

[†] This work was supported by research and equipment grants from the Israel Science Foundation, as well as by partial financial support of the U.S.−Israel Binational Science Foundation (Grant 2005270) and the EU (Grant MTKD-CT-2005-029936).

* To whom correspondence may be addressed. A.R.F.: e-mail, arf25@cam.ac.uk; tel, 0044 (0) 1223 402136; fax, 0044 (0) 1223 402140. E.H.: e-mail, haas@mail.biu.ac.il; tel, 00972-3-5318210; fax, 00972-3-7369928.

[‡] These authors contributed equally.

[§] MRC Center for Protein Engineering.

[||] Bar-Ilan University.

[1] Abbreviations: 22−55 distance, the distance between probes attached to residues 22 and 55; AEDANS, 1-aminoethylenediaminonaphthalene-8-sulfonic acid; BDPA, B domain of protein A; CD, circular dichroism; CI2, chymotrypsin inhibitor 2; ET, energy transfer; GdmCl, guanidinium chloride; HPLC, high-pressure liquid chromatography; MS, mass spectrometry; NATA, *N*-acetyltryptophanamide; SM-FRET, single-molecule fluorescence resonance energy transfer; tr-FRET, time-resolved FRET; WT, wild type.

10.1021/bi801890w CCC: $40.75 © 2009 American Chemical Society
Published on Web 02/17/2009

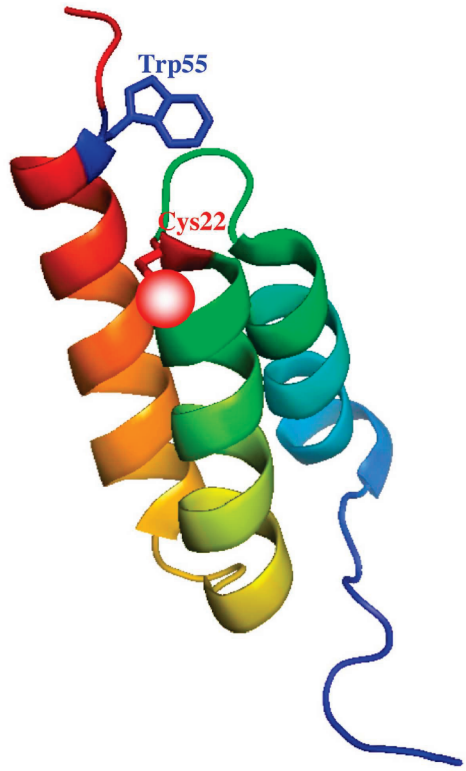

FIGURE 1: Structure of BDPA N22CA55W, derived from the wild-type NMR structure (PDB code 1SS1). The side chains of Cys22 and Trp55 were shown, and coumarin was shown as a red sphere. The image was created using PyMOL.

tr-FRET has been applied to measure the end-to-end distance distribution of short peptides and DNA and denatured and partially folded proteins, as well as protein domains (*16*−*18*, *22*−*27*). tr-FRET can also be applied to resolve subpopulations in ensembles of multiple conformers and distinguish the native and denatured states of two-state folding proteins (*28*). Here, we have applied tr-FRET to explore the ensembles of conformers of BDPA throughout its unfolding/refolding transition induced by change of GdmCl concentrations. To set up a tr-FRET system, we have introduced a Trp into BDPA at position 55 and a Cys residue at position 22, which was labeled with 7-acetamidocoumarin-4-carboxylic acid (I-coumarin) (Figure 1). The results of the global analysis of the tr-FRET experiments suggested that BDPA had two-state folding characteristics and its denatured state was compact at low concentration of GdmCl and expanded at higher concentrations of GdmCl.

MATERIALS AND METHODS

Protein Expression, Purification, and Labeling. BDPA gene was mutated by using QuikChange (Stratagene). The mutated BDPA was expressed in *Escherichia coli* and purified as described (*7*). In the labeling reaction, 50−100 μM BDPA was dissolved in phosphate buffer (20 mM phosphate, 150 mM NaCl, pH 7), and 1 mM tris(2-carboxyethyl)phosphine (TCEP) was added 10 min before the addition of a 10-fold excess of coumarin. The labeling reaction was carried out at room temperature and followed by matrix-assisted laser desorption/ionization time-of-flight mass spectroscopy (MALDI-TOF MS). After labeling, the free dye was quenched with β-mercaptoethanol, and the labeled protein was separated from the free dye with HPLC (Waters, Milford, MA) on a C8 column. Purified labeled protein was then lyophilized. HPLC and MS showed that the labeling efficiency was >98% for the purified protein. Analytical HPLC analysis confirmed the purity of the labeled protein samples (Supporting Information Figure S3). This supports the straightforward global analysis of the data in terms of distance distributions.

CD Measurements. In chemical denaturation experiments, the CD signal of 5 μM protein in NaOAc buffer (pH 5.7, 50 mM NaOAc plus 150 mM NaCl) at 222 nm was acquired at 25 °C on an Aviv spectrometer (Aviv Associates, Lakewood, NJ). Experiments on the temperature dependence of the CD signal were carried out on a J-815 CD sSpectrometer (JASCO, Tokyo, Japan) with 50 μM protein in NaOAc buffer (pH 5.7, 50 mM NaOAc plus 150 mM NaCl) at 222 nm.

Time-Resolved FRET Measurements and Data Analysis. (A) Preparation of Samples for Time-Resolved FRET Measurements. Lyophilized labeled BDPA samples were dissolved in 50 mM sodium acetate and 100 mM sodium chloride (pH 5.67) (buffer A). Protein concentration in the stock solutions was determined by the absorption spectrum. The extinction coefficients of BDPA (55W) and BDPA (55W, 22-coumarin) at wavelength 280 nm were 5700 and 7000 $L \cdot mol^{-1} \cdot cm^{-1}$, respectively. Stock guanidinium chloride solution was prepared in buffer A, filtrated by a 0.2 μm Millex-GN syringe driven filter unit (Millipore, Billerica, MA), and stored frozen at 0 °C. The guanidinium chloride concentration was determined by refractive index measurements using a Carl Zeiss 110623 refractometer (Nozaki 1972). GdmCl, UV grade, was purchased from ICN (Costa Mesa, CA).

(B) Time-Resolved FRET Measurements. The time-correlated single-photon counting method was used. The excitation source was a picosecond mode-locked Ti-sapphire laser (Tsunami; Spectra-Physics, Santa Clara, CA) pumped by a high-power diode laser (Millenia XsJ; Spectra-Physics, Santa Clara, CA) and equipped with broad-band optics. The laser output was frequency tripled by a flexible second and third harmonics generator (GWU; Spectra-Physics). The laser pulse width was 1.6 ps before doubling. A pulse selector (model 3980; Spectra-Physics) was used to reduce the basic 80 MHz pulse rate to 10 MHz. The donor fluorescence was excited at 297 nm. The emission wavelength was selected by a double $^1/_8$ m subtractive monochromator (DIGIKROM CM112, Albuquerque, NM) and directed to the surface of a cooled microchannel plate PMT (MCP-PMT; Hammamatsu 3809U-50, Albuquerque, NM) biased at −3200 V. The emission was collected at 350 nm (emission bandwidth 20 nm). A single-photon counting board (SPC 630; Becker and Hickel GmbH) fed via a preamplifier (HFAC-26DB 0.1UA, Brookline MA) and triggered by a photodiode (PHD-400N) was used. The response of the system yielded a pulse of full-width at half-maximum (fwhm) of 50 ps. The system was routinely checked for linearity and time calibration by determination of the decay kinetics of degassed anthracene in cyclohexane (Merck, NJ) (decay lifetime is 5.1 ns at 350 nm). The emission was collected with a polarizer at the magic angle (54.7°) relative to the excitation polarization. The reference excitation pulse profile used for deconvolution of the experimental decay curves was a scattered light pulse generated by placing a suspension of latex beads in the cell.

All measurements were done at 25 °C. Two fluorescence decay curves in each set of energy transfer (ET) experiments were measured. These were (a) the fluorescence decay curve of the Trp 55 residue in the absence of an acceptor in BDPA (55W) and (b) the fluorescence decay curve of the Trp 55 residue in the presence of the acceptor attached to the Cys 22 residue in BDPA (55W, 22-coumarin). The background emission was routinely subtracted from the corresponding fluorescence decay curve. To measure background emission, the buffer solution in the corresponding guanidinium chloride concentration was used. Donor emission was monitored at 350 nm (bandwidth, 20 nm). Data collection for each set of two measurements was done on the same day within a short time period. This reduced possible variations due to changes in calibration of instruments. Samples were routinely degassed and magnetically stirred during the measurement.

(C) Data Analysis. Average excited state lifetime was calculated by $\langle\tau\rangle = \sum_1^n \alpha_i\tau_i/\sum_1^n \alpha_i$ ($n = 3$), which is suitable for intensity averaging and in which τ_i stands for the lifetime components and α_i for their relative amplitudes. Average energy transfer efficiency, E, was calculated as $E = 1 - \langle\tau_{DA}\rangle/\langle\tau_{DO}\rangle$, where $\langle\tau_{DO}\rangle$ and $\langle\tau_{DA}\rangle$ stand for the average excited state lifetime of the donor in the absence and presence of an acceptor, respectively. Intramolecular distance distribution functions were obtained from simultaneous global analysis of the tryptophan emission decay curves obtained in the presence and the absence of the acceptor (*28*). Either the single-population model $p_0(r) = 4\pi r^2 e^{-b(r-a)^2}$ or the two-subpopulation model $p_0(r) = 4\pi r^2(frx(e^{-b_1(r-a_1)^2}) + (1 - frx)e^{-b_2(r-a_2)^2})$ was used as the model for determination of the radial intramolecular distance distribution, in which a_i and b_i are parameters proportional to the subpopulation's average and inverse of its standard deviation, respectively, and *frx* is the parameter which defines the fraction of the first subpopulation. The background emission was subtracted prior to the analysis. The evaluation of the quality of fit obtained by the curve fitting procedure was based on four indicators: the global χ^2 values, the distributions of the residuals, the autocorrelation of the residuals, and the error intervals of the calculated parameters (*29, 30*). The error intervals were obtained by a rigorous analysis procedure carried out for each set of experiments (*29*).

(D) Spectroscopic Measurements. Absorption spectra were measured on an Aviv model 17DS UV−vis IR spectrophotometer (Aviv Associates, Lakewood, NJ). Steady-state fluorescence spectra were recorded using an Aviv model ATF 105 fluorometer. The normalized spectral overlap integral, *J*, was determined as previously described (*31, 32*). The fluorescence emission spectrum of the tryptophan residue in BDPA (55W) was measured for each GdmCl concentration. The radiative lifetime of the donor (21.5 ns) was determined from measurements of the lifetime and the quantum yield of the tryptophan residue in the BDPA (55W) derivative. Quantum yield of the Trp residue in BDPA (55W) was calculated relative to that of a solution of degassed *N*-acetyltryptophanamide (NATA) in water, taken to be 0.13 (*33*). The value obtained for the tryptophan residue in BDPA (55W) in the absence of GdmCl was 0.073.

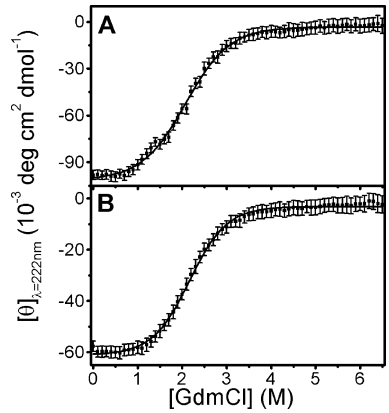

FIGURE 2: Far-UV CD detection of BDPA denaturation induced by GdmCl. (A) N22CA55W labeled by the coumarin probe ($[GdmCl]_{50} = 2.08 \pm 0.01$ M). (B) BDPA-N22CA55W (no acceptor) ($[GdmCl]_{50} = 2.16 \pm 0.01$ M). Data were acquired at 222 nm and 25 °C. Black dots indicate experimental results, and the black line indicates the sigmoidal nonlinear regression fit. The data were analyzed using Microcal's Origin data analysis software.

RESULTS

Protein Design and Stability. The BDPA used in this work was based on the Y15F mutant to remove the fluorescence from Tyr. We used Trp at position 55 as the FRET donor and 7-acetamido-4-coumarincarboxylic acid (coumarin) coupled to Cys22 as the FRET acceptor (Figure 1). This FRET pair has a Förster distance, R_0, of 24 Å. According to the NMR structure, the Cα−Cα distance between the wild-type residues 22 and 55 in the native state is only 9.2 Å. A very high FRET efficiency would be expected between the donor and acceptor labeled at positions 55 and 22, respectively, since the Förster distance for this donor/acceptor pair is larger than 20 Å. A large change of intramolecular mean distance between residues 22 and 55 should be detected upon denaturation, because they are separated by 32 residues. The protein stability was measured with CD spectroscopy before and after the attachment of the coumarin probe. This mutant was less stable (based on the CD-detected transition) than the wild type (WT), $[D]_{50\%}$ decreasing from 2.45−3.49 M GdmCl for the pseudo-WTs with Trp at other positions (3.49 M for Y15W, 2.45 M for N29HQ33W, and 2.95 M for E48W) (*6*) to 2.1 M GdmCl for this mutant. The coumarin-labeled and unlabeled mutants showed very similar stability ($[D]_{50\%} = 2.1$ M for both coumarin-labeled and unlabeled protein) (Figure 2), suggesting that the introduced coumarin does not interact with the protein or influence its folding pathway.

As a control, 1-aminoethylenediaminonaphthalene-8-sulfonic acid (AEDANS) and 5-acetamidosalicylic acid were also applied as FRET acceptor. Although they gave similar average distance as when coumarin acted as acceptor, these two FRET acceptors were not used in distance distribution analysis because the AEDANS has a long fluorescence lifetime, which is not perfect in distance distribution analysis (*28*), and Trp/salicylic acid has shorter Förster distance ($R_0 = 15$ Å), which is very suitable for the native state but too short for the denatured state of the protein.

Fluorescence Lifetime of Trp in the Absence of FRET. The fluorescence lifetime of the indole probe in proteins is a complex function of its interactions with the local environ-

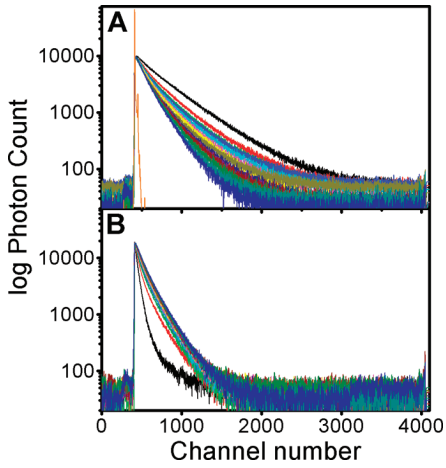

FIGURE 3: Time-resolved fluorescence decay traces of Trp emission in BDPA mutants. (A) BDPA-N22CA55W, no acceptor. (B) BDPA-N22CA55W (22-coumarin, A55W) with acceptor and hence with FRET at different concentrations of GdmCl. The time to channel ratio was 0.0122 ns/channel. GdmCl concentrations (M): 0.0, black; 1.7, red; 2.0, green; 2.1, blue; 2.25, cyan; 2.4, magenta; 2.5, yellow; 2.65, dark yellow; 2.75, navy; 2.8, purple; 2.9, wine; 3.0, olive; 3.5, dark cyan; 4.2, royal. The excitation pulse impulse response is shown in gold in panel A.

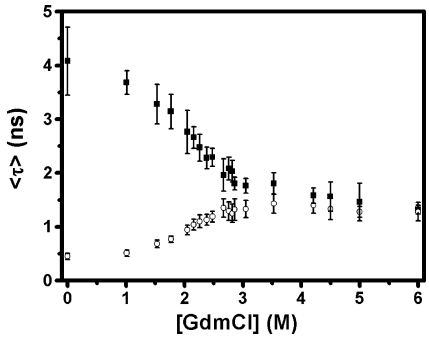

FIGURE 4: Averaged excited state lifetime of Trp55 in the absence (solid squares) and presence (open circles) of FRET at different GdmCl concentrations.

ment and the solvent. The fluorescence decay of the tryptophan residue 55 in the absence of an acceptor at residue 22 was measured under different GdmCl concentrations after the samples were degassed. A multiple exponential decay was observed (Figure 3), which is typical for Trp in proteins. Three lifetime components (ca. 5, 2, and 0.5 ns, Figure S1 in Supporting Information) commonly assigned to the three rotamers of the Trp residue were observed. The relative contribution of each component was dependent on the folding/unfolding conditions due to the protein's multiple local configurations and changes in the extent of solvent accessibility. The average excited state lifetime is plotted in Figure 4, which shows a significant decrease from ~5.2 ns in buffer to ~1.5 ns in 4.2 M GdmCl solution. The monotonic decrease of average excited state lifetime as a function of the denaturant concentration indicates increased quenching both from the solvent accessibility and possibly also from higher frequency of interaction with neighboring side chain and main chain chemical functions. Interestingly, the contribution of the long lifetime component, which was dominant at low GdmCl conentrations (below 1.8 M), was reduced under denturing conditions. At 4.2 M GdmCl the preexponents of the three lifetime components were nearly equivalent, but at higher denaturant concentration, e.g., at 6 M GdmCl, the long lifetime component (which was reduced to ~2 ns) was again dominant (54 ± 5%) probably due to preferential quenching of the more exposed rotamers. This change is consistent with earlier evidence of a structural change in the unfolded state due to the effects of GdmCl on BDPA (*9*). The long average lifetime of 5.2 ± 0.4 ns is considerably longer than the fluorescence lifetime of *N*-acetyltryptophanamide (NATA) (3 ns) under the same conditions. This is probably due to the slow exchange of the rotamer states and partial protection of Trp 55 from the solvent in the folded subpopulation of the protein.

Fluorescence Lifetime of Trp in the Presence of FRET. In the presence of FRET the fluorescence lifetime of the Trp residue decreased greatly (Figure 4). A 10-fold decrease under folding conditions, from 4.2 to 0.4 ns, resulted from the high efficiency of the energy transfer, $E = 0.89 \pm 0.02$, corresponding to an pseudoaverage distance of 15 ± 1.0 Å. With the addition of GdmCl, the average excited state lifetime of the Trp residue increased from 0.4 ns at 0 M GdmCl to 1.3 ns at 6 M GdmCl, concomitant with the strong increase of its fluorescence lifetime in the absence of the acceptor. Thus, the increase of the fluorescence lifetime was a clear consequence of the significant increase of the distance between the donor and the acceptor. The integrated transfer efficiencies under all solvent conditions were calculated using the average excited state lifetime of the donor in the absence and the presence of the acceptor. Both parameters showed a midtransition close to the concentration of 2 M GdmCl.

Global analysis of the decay curves of the donor emission in the presence and the absence of the acceptor yielded the distribution of the distance between the probes attached to residues 22 and 55 at each denaturant concentration. In this analysis, the fluorescence decay curves of the donor in the absence of the acceptor served as reference and internal standard, which accounted for the direct effect of the change of solvent and conformation on the donor lifetime. The Förster distance was also calculated for each case using this reference and the refractive index of the solvent, which is dependent on the GdmCl concentrations (*28*).

Determination of the Distribution of the Distance between Residues 22 and 55 by Global Analysis of tr-FRET Experiments. The global analysis of the fluorescence decay curves was based on a curve fitting algorithm and comparison of quality of fit to alternative models (*29, 30*). Multiexponential functions are ill-defined and can be fitted to several models (*34*). Most experimental decay curves, even those with low shot noise, can usually be perfectly fitted to a model of three, or sometimes four, discrete lifetime components. We chose to fit the data to models of continuous distributions since a model of three or four perfectly uniform populations is not a physical description of ensembles of protein molecules under partially folding conditions. The model that we used is flexible enough to accommodate the possible physical states, and since the FRET efficiency is not sensitive to both the low and the high extremes of the distributions, we based our conclusions mainly on the mean and the widths of the computed distance distributions. Here, we used statistical tests, in particular the examination of the autocorrelation of the residuals (*29, 30*), and compared the fit of the data to a model of single skewed Gaussian distribution and a model of sum of two skewed Gaussian distributions of the probability of the distance between the probes.

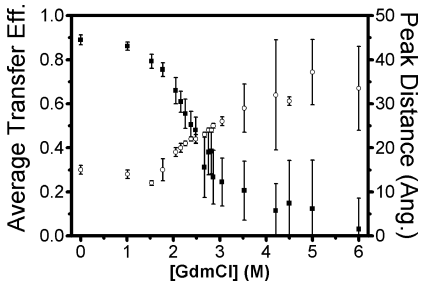

FIGURE 5: Average energy transfer efficiency (solid squares) and corresponding intramolecular distance distribution peak distance (open circles) obtained from analysis that assumes the single-population model in the transition zone.

Results of Global Analysis Using a Single-Population Model. Global analysis of the fluorescence decay curves of the donor obtained at full range of denaturant concentration at equilibrium was first done using a single-population model. This analysis yielded a series of distance distribution functions with expected characteristics of the chemically induced folding/unfolding transitions, mainly an unchanged native value of the mean distance up to the transition zone and then a monotonically increasing mean intramolecular distance (Figure 5). When a single conformational population was assumed, the peak position in the distance distribution shifted from ~15 Å at 0 M GdmCl to 30 Å at 4.2 M GdmCl and close to 35 Å at 5 M GdmCl.

The width of the distance distribution did not follow a monotonic change. The native state had a narrow distance distribution, which is expected for the ensemble of protein molecules in this state. Then slightly broader distribution at the pretransition zone and very broad distributions in the transition zone were observed. But, at the range of 2.5−3.0 M GdmCl, the global analysis again yielded narrow distributions, and only at higher GdmCl concentrations was the width broad as expected for ensembles of denatured protein molecules. That is, the mean distance was increased but the 22−55 distance in the ensemble of the denatured molecules was still well-defined. Interestingly, there seems to be a change in rotational freedom of the acceptor (under direct excitation) close to the point where this second folding transition starts (Supporting Information Figure S2). These results are interpreted as an indication of the contribution of residual, probably nonlocal, interactions that are still effective even after the main transition. At higher concentrations, these interactions are overrun by the stronger solvation by the denaturing solvent, and a major expansion of the denatured protein was observed.

The fact that the width of the distance distribution in the transition region was larger than both those of the native and the denatured ensembles is an indication of the coexistence of the two forms in the ensemble (Figures 6 and 7). Under appropriate conditions, the present experiment should enable a resolution of the two components as shown below. The increased uncertainty of the width of the distributions above 3 M GdmCl was probably due to the low observed transfer efficiencies (Figure 7). This was mainly due to the limits set by the Förster distance of the donor/acceptor pair used in the present experiments.

Distance between Residues 22 and 55 with Assumption of Two Populations. The next step was to apply an analysis based on a two-subpopulation model and compare the quality

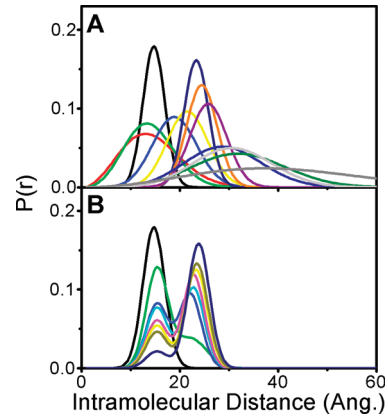

FIGURE 6: Distribution of the distance between residues 22 and 55 in BDPA at GdmCl concentrations between 0 and 5 M. (A) Results of data analysis assuming the single-population model for the intramolecular distance distributions of donor and acceptor (55W, 22-coumarin) in a series of GdmCl concentrations. (B) Results of data analysis assuming two subpopulations in the distribution of the intramolecular distance between residues 22 and 55 in the GdmCl concentrations for which this model was a better fitted one than the single population model. Key: black, 0.0 M; red, 1.0 M; green, 1.7 M; blue, 2.0 M; cyan, 2.1 M; magenta, 2.2 M; yellow, 2.3 M; dark yellow, 2.4 M; navy, 2.6 M; orange, 2.8 M; purple, 3.0 M; royal, 3.5 M; olive, 4.2 M; light gray, 4.5 M; gray, 5.0 M.

of fit obtained by the analyses using the two models. The main question in this step is how to extract the extra information, indicated by the increased width of the distance distribution found in the single-population model analysis of the transition zone measurements reported above. In order to do that, we reanalyzed the data sets obtained for the protein equilibrated in GdmCl concentration ranging from 1 to 2.6 M using the two-subpopulation model. At higher GdmCl concentration, the contribution of the native state is too small to be resolved with a high level of significance. In this analysis, the parameters for the native state were kept fixed to maintain a fixed number of degrees of freedom for the sake of statistical comparison (although the number of fitted points in a fluorescence decay is very large in comparison to the number of parameters in the model fitted. This is a reasonable assumption since the native state is not expected to change with GdmCl concentration and since at the range of distances well below the Förster distance the effect of small shifts of the mean distance on the transfer efficiency is small). The question at this point is whether the present experiments, with the current experimental noise level and small difference in the 22−55 distance in the two conformational states, could show statistically improved quality of fit. In the best fit model the residuals should be random, and therefore the residual's variance should be close to that when fitting the fluorescence decay curve with a multiexponential function. Therefore, the quality of fit was evaluated by two statistical criteria: (a) the autocorrelation of the residuals (which is a strong test for systematic deviations between the experimental data and the model) and (b) the χ^2 values and by two *F*-tests. The autocorrelation of the residuals showed clear preference for the two-subpopulation model for the midtransition GdmCl concentrations 2.0 M (Figure 7A) and 2.1 M. *F*-test comparison of the two models relative to a simple three exponential decay model also gave significant preference to the two-subpopulation model at these GdmCl concentrations with a significance level of $\alpha = 0.005$. For

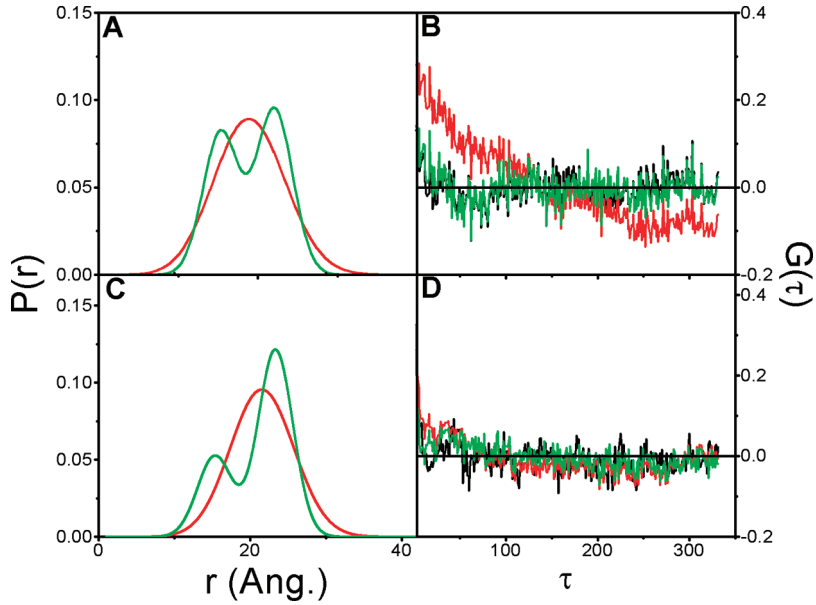

FIGURE 7: Comparison of the quality of fit of the tr-FRET experimental data using first a single-population model (red) and then using a two-subpopulation model (green). In panels A and C we show the calculated best fit distance distributions, and in panels B and D we show the autocorrelation of residuals of three analyses using the following models: The black trace for the lifetime analysis using a three exponential decay model. This analysis, which yields good fit of the data regardless of its physical meaning, gives a benchmark for the best possible fit of the current experimental decay curves. The red trace was obtained for the results of analysis for distribution of distances assuming a single population in the ensemble, and the green trace represents the autocorrelation of the residuals obtained for analysis of the same data sets assuming a two-subpopulation model. Panels A and B show the analysis for [GdmCl] = 2.0 M at the midpoint of the tr-FRET detected transition, and panels C and D show the analysis for [GdmCl] = 2.3 M. In panel B we see significantly better fit for the two-subpopulation model, while in panel D the difference is marginal and not considered significant.

the experiments done at 2.2−2.4 M GdmCl (where the denatured subpopulation was dominant) this *F*-test was positive for the two-subpopulation model with resolution at $\alpha = 0.05$ level. The *F*-ratio test, which compares the quality of fit of the two models, gave significant preference for the two subpopulations at all GdmCl concentrations between 2.0 and 2.4 M. Thus, on the basis of the graphs of the autocorrelation of the residuals and the *F*-tests, we can conclude that at the midtransition, where the mutant was equilibrated with 2.0 to 2.1 M GdmCl, the differences in the quality of fit were significant at the level which allows us to assert that there was an equilibrium between folded and denatured subpopulations of the protein molecules (Figure 7). As far as the intramolecular distance between residues at the two ends of the two native helices is concerned, there were two well-resolved ensembles at 2.0 and 2.1 M GdmCl, the folded molecules and the denatured molecules. This result supports the conclusion already deduced from other experiments that the chemical denaturation of BDPA is a two-state transition (*7, 9*).

The data obtained at GdmCl concentrations in the range from 0 to 1.7 M and from 2.6 to 6 M gave acceptable fits for both models. This protein has been studied using the single-molecule FRET detection where two subpopulations of transfer efficiencies were resolved at GdmCl concentrations between 2.5 and 3.5 M. The lower transition point observed here is due to the destabilization caused by the A22C mutation. The difference in stability prevents the direct application of the SM-FRET results as constraints in the analysis of the tr-FRET data. However, the two-state characteristics observed in the SM-FRET experiments are still a good constraint in the current data analysis where the one-population and two-population model cannot be distinguished with statistical measures mentioned above. We therefore analyzed the tr-FRET data obtained at 1−2.6 M GdmCl with the two-population model, and the results were presented in Figure 6B. The results show small variations in the mean and width of the distance distributions obtained for the two subpopulations and monotonically changing proportions of the two components when the GdmCl concentration increased (Figure 6B). At higher GdmCl concentration, not only the denatured state became more expanded, i.e., the mean distance increased, with GdmCl concentration but also the distance distribution width was also increased as expected for unordered states of heteropolymers (Figure 6A).

DISCUSSION

Distance Change upon Denaturation. BDPA is a three-helix bundle. Although positions 22 and 55 are separated by 32 residues in terms of primary sequence, they are very close to each other in tertiary structure with only 9.2 Å between Cα's (*7*). The FRET determined distance between fluorophores labeled at residues 22 and 55 was 15 ± 1 Å in the native state of BDPA. The longer distance is likely due to the linker between the fluorophores and the protein as well as the size of the fluorophores. This distance was unchanged at low GdmCl concentrations and only near the transition zone; i.e., at concentrations higher than 1.5 M, an increase consistent with the increase of GdmCl concentration was observed. A significant distance increase is expected if the H3 moves away from H2 upon denaturation. The distance increase proved the dissociation of H2 and H3. But, according to the two-population fitting, and even according to the single-population model analysis, in the denatured state at concentrations below 3.0 M GdmCl, the distance is only 22−24 Å in 1.7−2.6 M GdmCl, which is considerably smaller than expected for an unfolded polypeptide chain with

the same number of residues (*35*). The short distance of the denatured BDPA-labeled chain section could be the indication of nonlocal interactions in the denatured state or the existence of residual secondary structure.

One Population or Multiple Populations? The folding mechanism of BDPA has already been extensively investigated both experimentally and theoretically. Fast kinetics experiments supported a two-state folding mechanism (*7*). Single-molecule determination of FRET efficiencies also provided direct evidence for the existence of two major populations in the transition region (*9*). The added information from the tr-FRET experiments is the analysis of the FRET data in terms of distance distributions. The increased width of the distance distribution in the transition zone, relative to both the pre- and the posttransition zones of GdmCl concentrations, is a clear indication for multiplicity of conformational subpopulations. This is in support of the two-subpopulation analysis of the tr-FRET experiments. It should be noted that the $[D]_{50\%}$ for this BDPA mutant is around 2.0 M GdmCl, where both the native state and the denatured state were found to be equally populated. The current results show that at the folding/unfolding transition midpoint the two-subpopulation model is significantly preferred over that of a single population. The evidence for the existence of two distinct subpopulations, one native-like and the other denatured in the midtransition conditions, is a strong support for the barrier crossing (cooperative) mechanism of folding for this small fast-folding protein.

The Denatured State. Surprisingly, the denatured ensembles of BDPA molecules at GdmCl concentrations lower than 3 M, including the denatured subpopulations obtained in the transition zone, were characterized by a narrow distance distribution. This was in contrast to the distributions obtained at higher GdmCl concentrations and to the expected characteristics of unfolded proteins. Moreover, all the mean distances obtained by both models of analysis for the protein in GdmCl concentrations lower than 3 M were considerably lower than expected for a common 34-residue unstructured peptide. The narrow distributions with the short mean distances most probably represent a case of reduced intramolecular distances and small conformational space. The far-UV CD experiments showed that the secondary structure had almost disappeared at 3 M GdmCl, which does not support the existence of a considerable amount of secondary structure or native-like tertiary interactions. On the basis of these results we suggest that the population of denatured BDPA molecules at GdmCl concentrations below 3 M was compact mainly due to specific and perhaps some nonspecific nonlocal hydrophobic interactions. Similar hydrophobic interactions were also observed even at higher concentration of denaturant (*36, 37*). The experiments carried out at GdmCl concentration above 3 M yielded distance distributions with larger mean and width of distribution, indicating a looser ensemble of conformations with greater conformational space. This suggested that the nonlocal hydrophobic interactions in BDPA were gradually destroyed under stronger denaturing conditions. Similar observation was made in the single-molecule FRET study at high GdmCl concentrations, where the FRET efficiency for the unfolded state shifted from 0.3 to 0.2 when GdmCl concentration increased from 3 to 7 M (*9*).

Folding Mechanism. Φ-value analysis has suggested that BDPA folds through the nucleation−condensation model, where H2 folds first and acts as the nucleus in the transition state, although H3 was suggested to be more stable than H1 and H2 and might have residual secondary structure in the denatured state (*7, 38*). A compact denatured state of BDPA was also predicted by simulation (*38*). Our results further suggest that BDPA folds through a two-state mechanism, where the denatured molecules retain some nonlocal interactions up to 3 M GdmCl. A compact denatured state at low concentration of denaturant was also observed in other studies, which has been attributed to a hydrophobic collapse of the polypeptide chain (*39*−*41*). In temperature-jump experiments, only a single relaxation was observed (*7*). At high concentrations of denaturant, this compact ensemble gets gradually more expanded with the increase of GdmCl concentration. It is likely that the conformational change of the denatured state does not need to overcome considerable energy barrier (*20, 39, 42*) so that additional transitions were not observable in the T-jump experiments in GdmCl and its conformational change is just due to the change of the free energy profile of the denatured state with GdmCl. Single molecule techniques allow access to more information regarding the free energy profile of the denatured states (*20, 39*−*42*).

Single-Molecule versus Ensemble FRET Detection of Folding/Unfolding Transitions. It has been elegantly shown and reported that single-molecule FRET detection can resolve subpopulations of intramolecular distances based on the statistics of single-molecule transfer efficiencies. Huang et al. (*21*) studied the unfolding transition of BDPA and reported the resolution of two subpopulations of FRET efficiencies at GdmCl concentrations above ∼2.0 M. It should be pointed out that, so far, all single-molecule FRET experiments utilized probes with relatively long linker arm (13 Å for the pair used by Laurence et al.) and pairs with Förster distance larger than 50 Å which varies by about 10% over the denaturant concentration range (*41*). In the compact denatured and native states most molecules of any small single domain protein are expected to have intramolecular distances significantly smaller than that Förster distance. Therefore, most of the single-molecule FRET experiments which studied the folding/unfolding transitions of medium size globular proteins (L protein (*40*), cold shock protein (*42*), RNase H1 (*20*), CI2 (*41*), and BDPA (*9*)) cannot accurately determine the distance in the folded protein. It should be emphasized that in most current reports of single-molecule detected FRET experiments only transfer efficiencies were reported without calculation of distributions of distances because of the photobleaching and relatively high shot noise and the low time resolution (milliseconds). In the present report we show that ensemble trFRET is a powerful method for resolving subpopulations of intramolecular distance distributions and can provide more accurate distances than smFRET and therefore is a complementary technique of smFRET. Moreover, the time resolution of the trFRET experiment enables resolution of subpopulations that are separated by minimal (e.g., 2kT) activation energy barriers while the single-molecule FRET detection, where time resolution is limited by the low photon flux, cannot resolve subpopulations separated by such small barriers. The application of single-molecule FRET correlation and cross-correlation analyses (*20, 42, 43*) can cover the dynamics of

conformational changes in the range longer than the lifetime of the excited state of the donor, again complementing the trFRET approach.

In conclusion, this tr-FRET experiment supports the two-state model of folding of this small model protein and shows that up to medium GdmCl concentrations the denatured subpopulation retains nonlocal interactions that keep them compact.

ACKNOWLEDGMENT

The continuous technical support of Mr. Eli Zimermann is gratefully acknowledged.

SUPPORTING INFORMATION AVAILABLE

The change of the donor fluorescence lifetime with GdmCl in the absence and presence of acceptor (Figure S1), the fluorescence anisotropy properties of the donor and acceptor at different concentration of GdmCl (Figure S2), the HPLC analysis of labeled and unlabeled BDPA showing high purity (Figure S3), and the *F*-test (Table S1) and *F*-ratio test (Table S2) of the data analysis. This material is available free of charge via the Internet at http://pubs.acs.org.

REFERENCES

1. Mayor, U., Guydosh, N. R., Johnson, C. M., Günter Grossmann, J., Sato, S., Jas, G. S., Freund, S. M. V., Alonso, D. O. V., Daggett, V., and Fersht, A. R. (2003) The complete folding pathway of a protein from nanoseconds to microseconds. *Nature 421*, 863–867.
2. Fersht, A. R., and Daggett, V. (2002) Protein folding and unfolding at atomic resolution. *Cell 108*, 573–582.
3. Kubelka, J., Hofrichter, J., and Eaton, W. A. (2004) The protein folding "speed limit". *Curr. Opin. Struct. Biol. 14*, 76–88.
4. Dyer, R. B. (2007) Ultrafast and downhill protein folding. *Curr. Opin. Struct. Biol. 17*, 38–47.
5. Dimitriadis, G., Drysdale, A., Myers, J. K., Arora, P., Radford, S. E., Oas, T. G., and Smith, D. A. (2004) Microsecond folding dynamics of the F13W G29A mutant of the B domain of staphylococcal protein A by laser-induced temperature jump. *Proc. Natl. Acad. Sci. U.S.A. 101*, 3809–3814.
6. Sato, S., Religa, T. L., and Fersht, A. R. (2006) Phi-analysis of the folding of the B domain of protein A using multiple optical probes. *J. Mol. Biol. 360*, 850–864.
7. Sato, S., Religa, T. L., Dagget, V., and Fersht, A. R. (2004) Testing protein-folding simulations by experiment: B domain of protein A. *Proc. Natl. Acad. Sci. U.S.A. 101*, 6952–6956.
8. Sato, S., and Fersht, A. R. (2007) Searching for multiple folding pathways of a nearly symmetrical protein: Temperature dependent Phi-value analysis of the B domain of protein A. *J. Mol. Biol. 372*, 254–267.
9. Huang, F., Sato, S., Sharpe, T. D., Ying, L., and Fersht, A. R. (2007) Distinguishing between cooperative and unimodal downhill protein folding. *Proc. Natl. Acad. Sci. U.S.A. 104*, 123–127.
10. Lindorff-Larsen, K., Kristjansdottir, S., Teilum, K., Fieber, W., Dobson, C. M., Poulsen, F. M., and Vendruscolo, M. (2004) Determination of an ensemble of structures representing the denatured state of the bovine acyl-coenzyme A binding protein. *J. Am. Chem. Soc. 126*, 3291–3299.
11. Bertoncini, C. W., Jung, Y.-S., Fernandez, C. O., Hoyer, W., Griesinger, C., Jovin, T. M., and Zweckstetter, M. (2005) Release of long-range tertiary interactions potentiates aggregation of natively unstructured 336 {alpha}-synuclein. *Proc. Natl. Acad. Sci. U.S.A. 102*, 1430–1435.
12. Bouvignies, G., Bernadó, P., Meier, S., Cho, K., Grzesiek, S., Brüschweiler, R., and Blackledge, M. (2005) Identification of slow correlated motions in proteins using residual dipolar and hydrogen-bond scalar couplings. *Proc. Natl. Acad. Sci. U.S.A. 102*, 13885–13890.
13. Meier, S., Grzesiek, S., and Blackledge, M. (2007) Mapping the conformational landscape of urea-denatured ubiquitin using residual dipolar couplings. *J. Am. Chem. Soc. 129*, 9799–9807.
14. Wells, M., Tidow, H., Rutherford, T. J., Markwick, P., Jensen, M. R., Mylonas, E., Svergun, D. I., Blackledge, M., and Fersht, A. R. (2008) Structure of tumour suppressor p53 and its intrinsically disordered N-terminal transactivation domain. *Proc. Natl. Acad. Sci. U.S.A. 105*, 5762–5767.
15. Bernadó, P., Blanchard, L., Timmins, P., Marion, D., Ruigrok, R. W. H., and Blackledge, M. (2005) A structural model for unfolded proteins from residual dipolar couplings and small-angle x-ray scattering. *Proc. Natl. Acad. Sci. U.S.A. 102*, 17002–17007.
16. Haas, E. (2005) The study of protein folding and dynamics by determination of intramolecular distance distributions and their fluctuations using ensemble and single-molecule FRET measurements. *ChemPhysChem 6*, 858–870.
17. Ratner, V., Sinev, M., and Haas, E. (2000) Determination of intramolecular distance distribution during protein folding on the millisecond timescale. *J. Mol. Biol. 299*, 1363–1371.
18. Ratner, V., Amir, D., Kahana, E., and Haas, E. (2005) Fast collapse but slow formation of secondary structure elements in the refolding transition of *E. coli* adenylate kinase. *J. Mol. Biol. 352*, 683–699.
19. Magg, C., and Schmid, F. X. (2004) Rapid collapse precedes the fast two-state folding of the cold shock protein. *J. Mol. Biol. 335*, 1309–1323.
20. Kuzmenkina, E. V., Heyes, C. D., and Nienhaus, G. U. (2006) Single-molecule FRET study of denaturant induced unfolding of RNase H. *J. Mol. Biol. 357*, 313–324.
21. Huang, F., Settanni, G., and Fersht, A. R. (2008) Fluorescence resonance energy transfer analysis of the folding pathway of engrailed homeodomain. *Protein Eng. Des. Sel. 21*, 131–146.
22. Haas, E., Katchalski-Katzir, E., and Steinberg, I. Z. (1978) Effect of the orientation of donor and acceptor on the probability of energy transfer involving electronic transitions of mixed polarization. *Biochemistry 17*, 5064–5070.
23. Sahoo, H., Roccatano, D., Zacharias, M., and Nau, W. M. (2006) Distance distributions of short polypeptides recovered by fluorescence resonance energy transfer in the 10 Å domain. *J. Am. Chem. Soc. 128*, 8118–8119.
24. Möglich, A., Joder, K., and Kiefhaber, T. (2006) End-to-end distance distributions and intrachain diffusion constants in unfolded polypeptide chains indicate intramolecular hydrogen bond formation. *Proc. Natl. Acad. Sci. U.S.A. 103*, 12394–12399.
25. Parkhurst, L. J. (1995) Donor-acceptor distance distributions in a double-labeled fluorescent oligonucleotide both as a single strand and in duplexes. *Biochemistry 34*, 293–300.
26. Amir, D., and Haas, E. (1988) Reduced bovine pancreatic trypsin inhibitor has a compact structure. *Biochemistry 27*, 8893–8889.
27. Li, B., Phillips, N. B., Jancso-Radek, A., Ittah, V., Singh, R., Jones, D. N., Haas, E., and Weiss, M. A. (2006) SRY-directed DNA bending and human sex reversal: reassessment of a clinical mutation uncovers a global coupling between the HMG box and its tail. *J. Mol. Biol. 360*, 310–328.
28. Haran, G., Haas, E., Szpikowska, B. K., and Mas, M. T. (1992) Domain motions in phosphoglycerate kinase—Determination of interdomain distance distributions by site-specific labeling and time-resolved fluorescence energy-transfer. *Proc. Natl. Acad. Sci. U.S.A. 89*, 11764–11768.
29. Beechem, J. M., and Haas, E. (1989) Simultaneous determination of intramolecular distance distributions and conformational dynamics by global analysis of energy transfer measurements. *Biophys. J. 55*, 1225–1236.
30. Grinvald, A., and Steinberg, I. Z. (1974) On the analysis of fluorescence decay kinetics by the method of least-squares. *Anal. Biochem. 59*, 583–598.
31. Amir, D., and Haas, E. (1987) Estimation of intramolecular distance distributions in bovine pancreatic trypsin inhibitor by site-specific labeling and nonradiative excitation energy-transfer measurements. *Biochemistry 26*, 2162–2175.
32. Beals, J. M., Haas, E., Krausz, S., and Scheraga, H. A. (1991) Conformational studies of a peptide corresponding to a region of the C-terminus of ribonuclease A: implications as a potential chain-folding initiation site. *Biochemistry 30*, 7680–7692.
33. Das, T. K., and Mazumdar, S. (1995) pH-induced conformational perturbation in horseradish peroxidase. Picosecond tryptophan fluorescence studies on native and cyanide-modified enzymes. *Eur. J. Biochem. 227*, 823–828.
34. Lanczos, C. (1956) *Applied Analysis*, Prentice Hall, Engelwood Cliffs, NJ.
35. Brant, D. A., and Flory, P. J. (1965) The configuration of random polypeptide chains. I. Experimental results. *J. Am. Chem. Soc. 87*, 2788–2791.

36. Saab-Rincón, G., Gualfetti, P. J., and Matthews, C. R. (1996) Mutagenic and thermodynamic analyses of residual structure in the alpha subunit of tryptophan synthase. *Biochemistry 35*, 1988–1994.
37. Neri, D., Billeter, M., Wider, G., and Wuthrich, K. (1992) NMR determination of residual structure in a urea-denatured protein, the 434-repressor. *Science 257*, 1559–1563.
38. Alonso, D. O. V., and Daggett, V. (2000) Staphylococcal protein A: Unfolding pathways, unfolded states, and differences between the B and E domains. *Proc. Natl. Acad. Sci. U.S.A. 97*, 133−138.
39. Schuler, B., Lipman, E. A., and Eaton, W. A. (2002) Probing the free-energy surface for protein folding with single-molecule fluorescence spectroscopy. *Nature 419*, 743–747.
40. Sherman, E., and Haran, G. (2006) Coil-globule transition in the denatured state of a small protein. *Proc. Natl. Acad. Sci. U.S.A. 103*, 11539–11543.
41. Laurence, T. A., Kong, X., Jäger, M., and Weiss, S. (2005) Probing structural heterogeneities and fluctuations of nucleic acids and denatured proteins. *Proc. Natl. Acad. Sci. U.S.A. 102*, 17348–17353.
42. Nettels, D., Gopich, I. V., Hoffmann, A., and Schuler, B. (2007) Ultrafast dynamics of protein collapse from single-molecule photon statistics. *Proc. Natl. Acad. Sci. U.S.A. 104*, 2655–2660.
43. Haas, E., and Steinberg, I. Z. (1984) Intramolecular dynamics of chain molecules monitored by fluctuations in efficiency of excitation energy transfer. A theoretical study. *Biophys. J. 46*, 429–437.

BI801890W